COBEM 2021 26th International Congress of Mechanical Engineering
ABCM Associação Brasileira de Engenharia e Ciências Mecânicas
November 22-26, 2021, Virtual Congress, Brazil

COBEM2021-2061

RAPID SCALE PROTOTYPING TECHNIQUE FOR A MINI MAGNETIC COOLER STUDY DEVELOPMENT

Edigar Junior Schumacker Botelho
Julio Cesar Guimarães Tedesco
Lucas Venancio Pires de Carvalho Lima
Polytechnique Institute of Rio de Janeiro State University (IPRJ/UERJ), Rua Bonfim 25, Vila Amélia, Nova Friburgo - RJ, CEP 28625-570, Brazil.
edigar.uerjlab@gmail.com, tedesco.jcg@gmail.com, lucaslima.iprj@gmail.com.

Abstract. *A small-scale prototype magnetic cooler is being developed using 3D modeling and rapid prototyping by a 3D printer. Several simplified tests were performed to evaluate different systems before the construction. Initially, some mechanical elements of the project were studied, such as the structural components. The main parts of the system are: a gear where two sectors of magneto-caloric material are placed, two bearings that are also used to place the four permanent magnets and the shaft. These sectors will be built by Gadolinium wires, which exchange heat with the water running through the entire refrigeration circuit. Among the instrumentation techniques adopted to verify ranges of safety and efficiency parameters are the leakage test of the sealing element underwater pressure and the friction test between the retainer and the shaft, which made it possible to measure the forces against the movement of the gear (driven by a stepper motor through a timing belt). Finally, structural simulations using finite element software were made to guarantee a minimum deformation of the prototype and verify stresses in the components. These simulations provide information that guarantees that there would be no risk of fracture or alteration of dimensional parameters. As a result of the tests, it was possible to acquire enough data to proceed with the assembly and manufacture of the other components of the magnetic refrigerator prototype.*

Keywords: *Magnetic Refrigeration, Design, 3D printer.*

1. INTRODUCTION

Among the electrical and electronic devices present in a home, the refrigerator is one of the most indispensable. The main temperature control parameter of a conventional refrigerator is the pressure of the gas flowing in the ducts of the compartments. One of the advantages of conventional refrigerators is the ease of manufacture and availability of raw material for their structural and functional components, making the appliance an affordable consumer good. On the other hand, the conventional refrigerator brings problems to the environment, due to its working fluid, the compound called HFC, being highly contributor to global warming (Benhadid-Dib and Benzaoui, 2012), with the emissions being caused in the production, repair and disposal of refrigerators (Calm, 2002).

A solution to this problem may lie in changing the technology adopted in refrigerators (Kitanovski *et al*., 2015). The magneto-caloric effect (MCE) could be a more efficient technology that is less harmful to the environment (Smith, 2013). Roughly speaking, MCE is associated with the ability of a material to change its temperature with the variation of the external magnetic field (Tishin and Spichkin, 2014). There are two physical quantities used to characterize the MCE: the adiabatic temperature change (ΔT) and the isothermal entropy change (ΔS). In addition, the efficiency of the magnetic refrigerator is larger than common refrigerators (Kitanovski *et al.*, 2015). However, there are still some disadvantages to overcome, such as the high price of materials used as coolants and the difficulties to produce a sufficiently strong magnetic field to obtain a suitable MCE for the application (Gschneidner and Pecharsky, 2008). Despite these challenges, a few prototypes using MCE can already be found.

In 1978, Brown and later Steyert built the first two prototypes of magnetic coolers that operated close to room temperature, using Gadolinium metal (Gd) as the refrigerant material (Gschneidner and Pecharsky, 2008), that continues to be the most popular material for prototype construction (Thishin, 2003), since it is commercially available (Dankov et al., 1998). Further developments evaluated different refrigerator parameters (Lozano, 2016). The magnetic field can be produced by permanent magnets or coils with electric current (Gschneidner and Pecharsky, 2008).

Among the many magnetic refrigeration systems, also called active magnetic regenerators (AMR), one of them is the rotary refrigerators (Tušek *et al.*, 2010). Despite presenting several challenges, when compared to reciprocating compressors refrigerators, this kind of system also presents several advantages and useful properties (Vuarnoz *et al*., 2011). For this reason, it is relatively easy to find works related to this type of system (Albertini *et al.*, 2017, and Huang

et al., 2019).

Polymers are among the most used materials since they have useful characteristics in several areas (Dias, 2011). In the current scenario, polymers gain space in various segments, such as household utensils, engineering projects, electronics, construction material, packaging, among others, and can be produced in complex forms through additive manufacturing, enabling greater alternatives in industries at the prototype design stage (Kurek, 2009).

In this context, polymers have gained greater importance with the development of additive manufacturing by the availability of 3D printers. It is worth noting that printed parts can be useful in engineering applications that require good corrosion resistance and low density (Galina, 2016, Shang, 2020, and Szykiedans, 2017). The low cost of 3D printing devices and supplies, added to the ability to print complex geometries of high-value products, have made them economically attractive (Wittbrodt, 2013).

There are three types of polymers easily commercially available for rapid scale prototyping: PLA, polylactic acid, or polylactide; ABS, Acrylonitrile Butadiene Styrene; and PETG, a Glycol Modified version of Polyethylene Terephthalate (Szykiedans, 2017). Each of them has advantages and disadvantages (Martinez, 2019). Among the advantages of PLA we can mention better surface finishing, less deformation of printed parts, faster prototyping, and greater tensile strength. However, these properties do not guarantee the necessary hydraulic sealing of the device. For this reason, there is a need to machining the parts after printing, in addition to the use of sealing elements that guarantee the absence of leaks (Martinez, 2019, Divyathej, 2016, and Anitha, 2001).

This work proposes to describe the development of a mini-refrigerator based on the magnetocaloric effect. Gd was chosen as the refrigerant material. In order to keep a low cost and a small size, a set of commercially obtained permanent magnets was used to generate the magnetic field. In addition, a 3D printer was used to produce the main parts of this AMR, made with ABS. The text that follows intends to present the analysis of the physical and mechanical properties of the main components of the refrigerator, as they are part of the study needed to build the device.

2. THE THERMOMAGNETIC BRAYTON CLOSED CYCLE

The operation of a magnetic cooler is based on the MCE. The idea is to use the temperature variation in the regenerator material, which is produced by changing the magnetic field, to compose a closed thermodynamic cycle. Figure 1 (a) presentes the thermal response of Gd metal, which is the material used as a regenerator. With the peak positioned very close to the magnetic transition temperature of Gd ($T_C \cong 295\ K$), the $\Delta T\ vs.\ T$ has a maximum amplitude around $1.2\ K$ for a field variation of $\Delta B = 0.25\ T$ (Tishin, 2003).

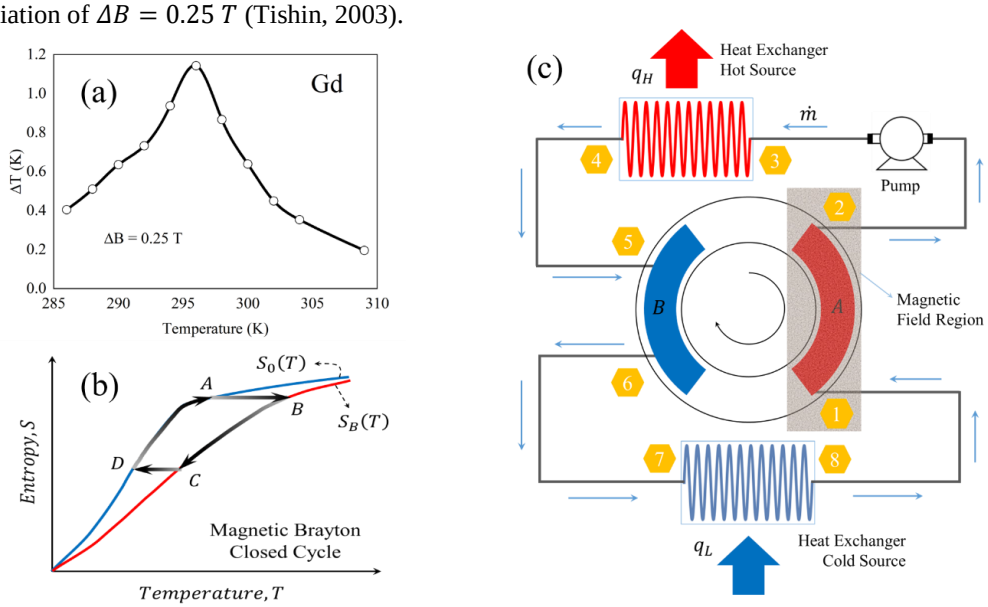

Figure 1. (a) Magnetic response of Gd under $\Delta B = 0.25\ T$. (b) The magnetic Brayton cycle ABCD using entropy functions $S_B(T)$ and $S_0(T)$ for with and without B. (c) Schematic diagram of the magnetic refrigerator indicating the points of entrance and exiting of fluid (from 1 to 8), the heat exchangers and the heat flux rate q_H and q_L.

A typical cycle for this type of device is the Brayton cycle (Tishin, 2003). This closed loop (Figure 1.b) consists of two isentropic processes (constant entropy) and two isofield processes (constant magnetic field). Starting from state A, a magnetic field is applied to the magnetic material. In an isentropic process, its temperature increases until state B. At this moment, a constant magnetic field process takes place and the heat is removed from the material, which takes it to state C. Afterwards, the magnetic field is taken away and the material has its temperature decreased until it reaches point D in a constant entropy process. Finally, again in a process with constant magnetic field, the material absorbs heat up to the initial state A. This thermomagnetic closed cycle can be applied using the scheme shown in Figure 1(c).

A relatively uniform magnetic field is generated by permanent magnets. When sector A of Gd enters this region, its temperature is increased as described above. At the same time, a fluid composed of a mixture of water with alcohol and mass rate $\dot{m}$, supplied by a pump, percolates the sector removing heat from the magnetocaloric material, characterizing the isofield process also described above. After passing through the magnetized material, the fluid loses heat in the heat exchanger of the hot source (Figure 1.c). After a certain time, sector A leaves the magnetic field region and its temperature is reduced. Concomitantly, the other sector of Gd (sector B) that has already gone through these thermodynamic processes, at a lower temperature, is thermally interacting with the fluid that has already passed through the hot source heat exchanger. This causes a reduction in the fluid temperature. Thus, when the fluid passes through the cold source heat exchanger, it can absorb heat, making the system act as a cooler regime. Finally, this same fluid passes through sector A again, closing the thermomagnetic cycle.

3. ROTARY SYSTEM OF THE MAGNETIC COOLING

In the present work, the project of a prototype will be presented, which is being developed using a 3D CAD software and which principal components will be built by means of rapid prototyping. To ensure the feasibility of the model, initial analysis was carried out. The main elements of the project can be seen in figure 2.

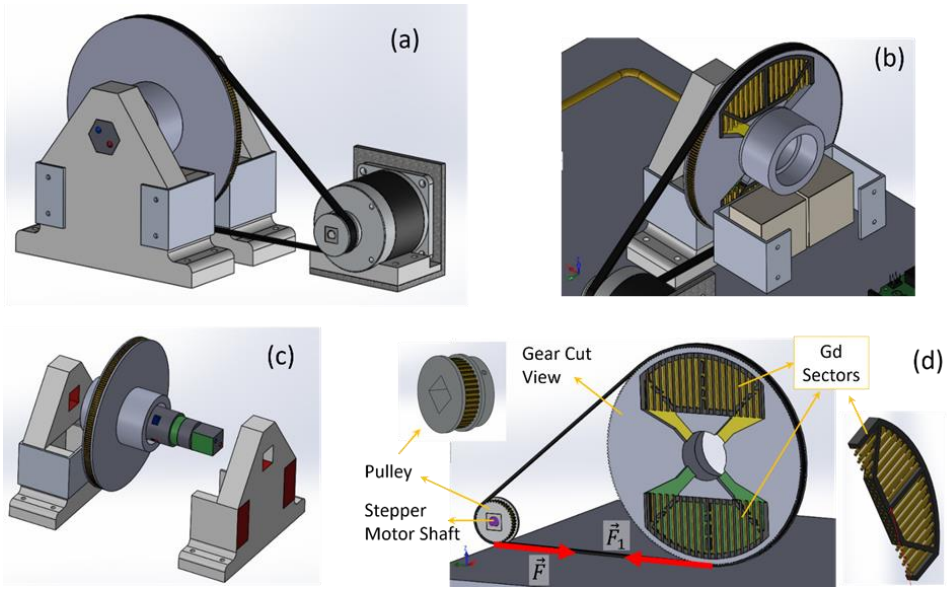

Figure 2. (a) Perspective view of the prototype, showing the stepper motor, bearings, the timing belt and a gear. (b) Perspective view of the prototype without one of the bearings and without the shaft to show one of the permanent magnet pairs in detail. (c) Exploded view of the prototype. (d) Detailed view of the gear and pulley.

One of the main elements of the system is a gear where two sectors of magnetocaloric material are placed (figure 2.d). These sectors are formed by Gd wires (Ø = 1.5 mm) with the function of exchanging heat with the mixture of water + alcohol that runs through the entire refrigeration circuit. This gear will rotate around a shaft with holes (figure 2.c) that has the function of directing the fluid to the internal sectors of the gear to perform the heat exchange (figure 6.c). These holes match the gear fluid inlets and outlets in two distinct gear positions. Rotation of the gear is possible due to two bearings that connect the gear to the shaft. For sealing, commercial retainers were chosen. The shaft is fixed in two supports (figure 2.c) which are also used to house four magnets, which produce the necessary magnetic field to induce the magnetocaloric effect. A water pump generates the flow of the water + alcohol mixture.

Four commercially available permanent magnets were used (grade N48, Nd-Fe-B alloy). The dimensions of the other components were defined from such available magnets (Table 1). The choice of bearings and retainers was related to the availability. In order to facilitate the rotation of the gear around the shaft, ball bearings were used (SKF 6805). To prevent leakage in the system, simple gasket retainers (BRG Nitrile) were used. The supports of the system will be printed in 3D. To fix permanent magnets to the supports, an aluminum plate (Al) 1100 was considered (Figure 2.a).

Table 1. Main used dimension of the project parts.

Parts	Dimension values
Permanent Magnets	Pole area $(40 \times 40) \times 10^{-6}\ m^2$ and thickness $20 \times 10^{-3}\ m$
Gear	Diameter $131.25 \times 10^{-3}\ m$
Toothed Pulley	Diameter $25.50 \times 10^{-3}\ m$
Ball bearings	$External\ diameter\ = 37 \times 10^{-3}\ m\ and\ Internal\ diameter\ = 25 \times 10^{-3}\ m$
Gasket retainers	$External\ diameter\ = 37 \times 10^{-3}\ m\ and\ Internal\ diameter\ = 25 \times 10^{-3}\ m$

The stepper motor presents a circular geometry and is fixed in a L-profile plate in order to ensure its stability in operation (figure 2a). The hydraulic system that irrigates the entire system passes through the shaft that supports the gear, having two holes that run axially along the shaft (figure 2a) to the radial holes (figure 2c) that distribute the fluid through the gear allowing heat transfer. The heat exchangers consist of copper coils, they are not shown in the figure.

The magnetic material will consist of Gd wires and will be housed in two sectors in the gear (Figure 2.b and Figure 2.d). To fix their position within the sector space, a frame will be 3D printed (Figure 2.d). While the cooler operates, the shaft remains static while the gear rotates on it, through the bearings. The square geometry of the shaft cross section in figure 2(c) is due to a simplification performed specifically to decompose the forces imposed on the system in the structural analysis.

Forces F_1 and F form the action-reaction pair in the gear and the motor pulley (figure 2.d). The maximum torque of the NEMA 23 stepper motor is specified by the manufacturer and is related to its operating angular speed. A low angular speed of 1.7 Hz was chosen. At this frequency, the motor provides a maximum torque of $|\tau| = \tau = 0.45\ N \cdot m$ (NEOMOTION). The maximum force F_1 that the motor can exert, from the specified torque, can be calculated with the pulley radius. As the gear force F_1 is the reaction pair of pulley force F, due to tension on the timing belt, it is possible to calculate the maximum torque that can be generated by the motor in relation to the center of the gear.

$$F\ r_{pulley} = \tau_{motor} \quad \text{and} \quad F_1\ r_{gear} = \tau_{gear} \quad \rightarrow \quad F(max) = F_1(max) = 35.37\ N$$

$$\tau_{gear} = (\tau_{motor}/r_{pulley})\ r_{gear} = 2.32\ N \cdot m \tag{3}$$

To determine some necessary parameters and their safety ranges, instrumentation techniques were adopted. One of these is the leakage test of the sealing element under water pressure, the retainer. Leaks in the system can damage prototype components and emptying the water tank would make the heat exchange system difficult. Another test performed was the evaluation of friction between the retainer and the shaft, which enabled the measure of friction resultant forces against the movement of the gear. A stepper motor, connected to it by a timing belt, carries out the movement of the gear. In addition, finite element methods were used to verify structural resistance. As a result of these tests, it was possible to acquire enough data to proceed to the manufacture and assembly of the magnetic refrigerator prototype.

3.1 **Friction Force and Leak Test**

To obtain the amplitude of the real force exerted in this system, it is necessary to estimate friction forces. Among these, the friction resulted from the gasket and bearings on the shaft. In order to perform an experimental evaluation, a simple 3D printed system was set up (Figure 3.a). This system consists of a part of the shaft and a part of the gear, where one gasket-bearing assembly is mounted, fixed by two 3D printed supports. In order to evaluate several lever arms, a rod with holes was coupled to the system. Knowing the applied mass and its lever arm R, it was possible to make a linear adjustment ($mass\ vs. \frac{1}{R}$) thus obtaining the resistance-related force of the system using one gasket-bearing pair, $0.172\ N \cdot m$. Remembering that this analysis is for a seal-bearing pair, the result must be duplicated to meet the prototype ensemble. Thus, the necessary force to overcome the static friction between these two elements, using the lever arm equivalent to the radius of the prototype gear, is equal to $|F_{at}| = F_{at} = 5.82\ N$.

In order to verify the pressure that the gasket would withstand without leaking at its interface with the 3D printed shaft, a specific hydraulic system was constructed (figure 3b). The built-in system makes it possible to apply pressure through a low-cost, easy-to-use hospital syringe. A pressure sensor ($1.2\ MPa$, SEEED-G1/4) was coupled to the system, which interfaces with an Arduino UNO board. Sensor calibration was performed using a water column pressure with known heights. Results obtained show that the pressure varies linearly with the signal (voltage reading by Arduino).

Once the system was calibrated, a range of pressure was applied to the system, there was no evidence of leakage in the contact between the elements with operating gauge pressures (approximately $30\ kPa$).

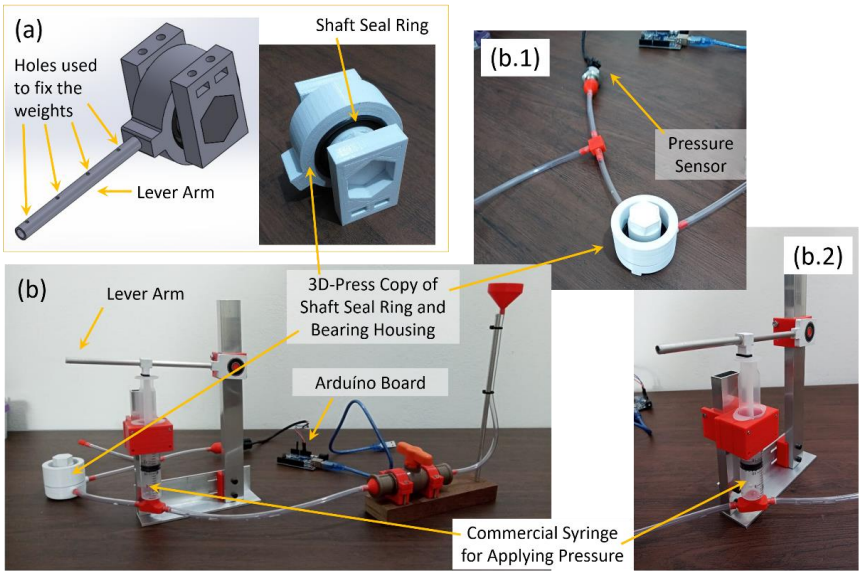

Figure 3. (a) Friction test assembly (b1) Simplified test of leakage between shaft and gear (b) Complete model of the specific hydraulic system (b2) System to apply pressure.

3.2 **Magnetic Forces**

The forces due to interactions with the magnetic field were estimated using the *femm* software (Finite Element Method Magnetics). The sectors of Gd, bearings and permanent magnets were considered. Although these analyzes are only in 2D planes, it is possible to specify the depth of the elements in the problem. The Al-1100 plates that fix the permanent magnets were also represented, even though Al is a diamagnetic element. Two simulations were performed, simulation 1 being a top view of the set and simulation 2 related to a side view of the set. The following assumptions were made:

- The Gadolinium sector is composed of wires ($\emptyset = 1 \times 10^{-3}\ m$), but for simplification, it was considered as a solid. In both simulations, the dimensions of Gd in the simulation planes were defined by the real dimensions, while the dimension perpendicular to the simulation plane was defined in order that the equivalent parallelepiped had the total mass of a massive sector of Gd;
- Using the same simplification, parallelepipeds made of iron (Fe) were considered to represent the bearings (figure 4-b).

In both cases, the amplitude of the magnetic field flux was compatible, $|B| \cong 0.6\ T$. Furthermore, the fields showed relative uniformity in the region between the magnets. This is desired for the study and prediction of the magnetocaloric effect (Tishin, 2003).

The attraction and repulsion forces between the permanent magnets could be calculated by simulation 1. The attraction force between the two pairs of magnets on the left and the two pairs of magnets on the right is given by $|F_{ch}| = 234.65\ N$.

The calculated interaction force between the sector of Gd and the set of four permanent magnets was approximately null, due to the symmetry of the system. The magnetic force calculated on the Gd sector in the region with the strongest magnetic field, described by F_{i-sG}, has an amplitude equal to $10.69\ N$ pulling the Gd sector down $(-z)$.

The F_m force resulted from the interaction between the magnets and the gadolinium sectors. Taking as reference the vertical direction (Figure 4.a), several positions of the Gd sector were evaluated, representing different configurations in which the sector will pass in the cyclical operation of the refrigerator.

This analysis serves to ascertain the magnetic force due to the magnetic field gradient. Forces related to eddy currents were disregarded, as the sectors are actually formed by wires positioned perpendicularly to the field lines. In addition, the effects due to variations in the magnetic flux caused by the variation in position by the Gadolinium sector were also disregarded. Thus, the maximum value obtained for this force was $|F_m| = 36{,}67\ N$.

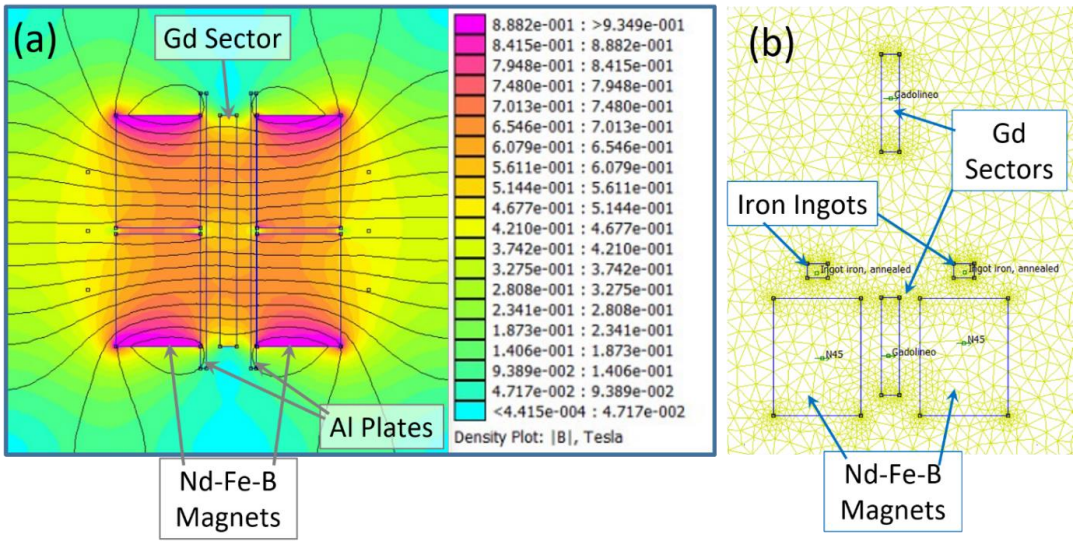

Figure 4. (a) Simulation 1 - Top view showing the set of permanent magnets (two pairs on each side), two Al plates and the equivalent sector of Gd. (b) Simulation 2 - Side view showing two equivalent sectors of Gd, two parallelograms of iron representing the two bearings and the two permanent magnets with depth equivalent to the pairs of magnets.

To obtain the torque caused by the total magnetic force ($|\tau_m| = \tau_m$), the central position of the sectors in relation to the gear center is taken into account, $d_{sector} = 0.0423\ m$. Thus,

$$|\tau_m| = \tau_m = F_m\, d_{sector}$$

$$\tau_m = 1.538\ N \cdot m \tag{4}$$

Therefore, considering the torque relative to the friction force, $|\tau_{gear}| = \tau_{gear} = 0.344\ N \cdot m$, according to Equation (3), and the magnetic torque calculated above, $\tau_m = 1.538\ N \cdot m$, it is possible to calculate the maximum torques contrary to the motor movement of step, $\tau_1 = |\tau_1|$:

$$\tau_1 = \tau_m + \tau_{gear} = 1.882\ N \cdot m \tag{5}$$

Thus, it is concluded that the maximum F_1 force required for the motor to move the system with constant angular velocity is:

$$|F_1| = F_1 = 8.71\ N \tag{6}$$

3.3 **Forces on Gear, Shaft and Bearings**

Once the magnetic interaction forces between the elements of the system are known, and considering the weight of each part of the system, it is possible to determine the forces acting on each of these parts.

The F_{i-sG} force is caused by the interaction between the magnets and the Gd sector immersed in the most intense region of the magnetic field (Figure 5b). The reaction forces F_{ry} and F_{rz} (Figure 5.b) are calculated from the equilibrium of forces in the respective $y$and $z$axes ($|F_{rey1}| = F_{rey1} = 7.96\ N$ and $|F_{erz}| = F_{erz} = 14.38\ N$).

The force F_{peng} is the weight force of the gear coupled with the Gd sectors, this value being equal to $|F_{peng}| = F_{peng} = 3.69\ N$. The F_1 is $65.625 \times 10^{-3}\ m$ away from the gear center.

The shaft is coupled inside the gear through the bearings in the green circular region (Figure 5.a). There is contact between the shaft and the 3D printed supports in the green square region (Figure 5.a). The reaction forces that the gear causes on the bearings, which in turn have their reaction on the shaft, can be calculated from $\frac{F_{ry}}{2}$, since it is being distributed on two symmetrical and identical surfaces. Hence, $|F_{rol}| = F_{rol} = 3.98\ N$. Forces in the y direction (F_{rey1} and F_{rey2}) are evenly distributed on the surfaces in the two red square regions in contact with the 3D printed supports, because the geometry is symmetric. That is, $F_{rey1} = F_{rey2} = 3.98\ N$.

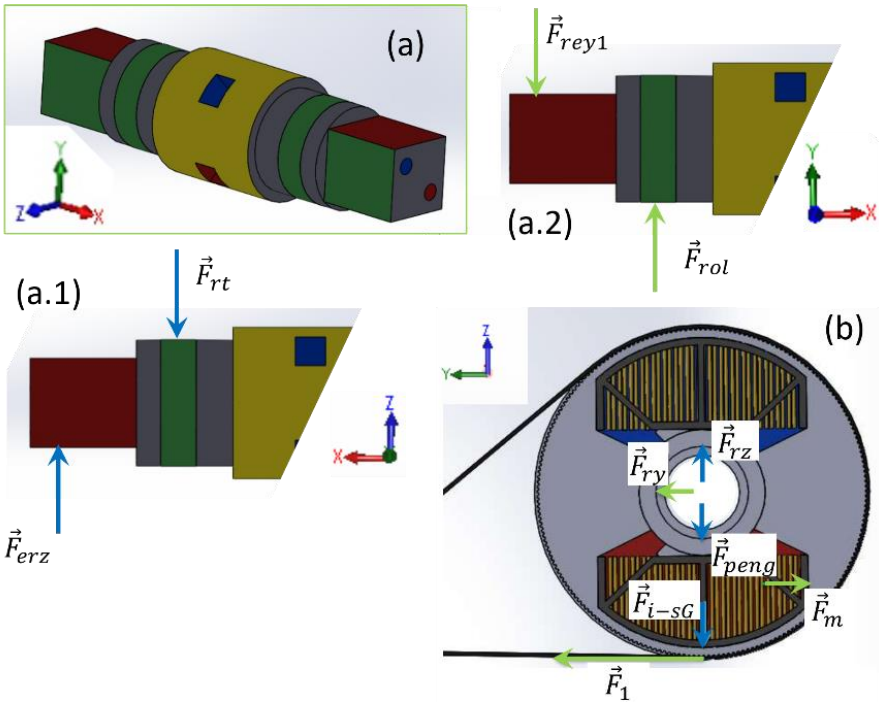

Figure 5. (a) Shaft isometric view. (a.1) Forces in the XZ plane (a.2) Forces in the XY plane (b) Forces in the XZ plane.

The forces on the z axis, illustrated in Figure 6(b), are composed of the weight of the shaft (P_{zeix}), calculated in SolidWorks software, and the weight of the bearings (P_{zrols}) and gaskets (P_{zrets}), measured on the precision scale (SF-400 model).

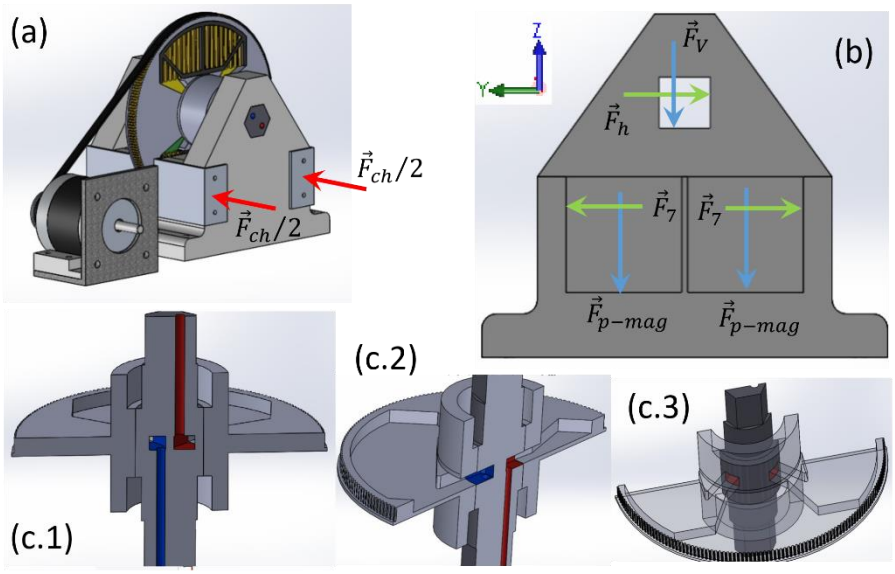

Figure 6. (a) Forces in the X direction (b) Forces in the YZ plane (c) Representation of the internal ducts on the shaft.

The sum of these mentioned weight components is called F_{pz}. Another contribution to the force on the z-axis is the reaction force (F_{rez}), in addition to the F_{i-r} which is the force of the magnet's interaction with the bearings. The force caused by the interaction of the magnet with the bearings was calculated with the 2D analysis using the *femm* (21.8 N).

The variable F_{rt} is the sum of the forces acting in the region of contact with the bearing, so F_{rt} is equivalent to the contribution of F_{rz}, $\frac{F_{pz}}{2}$ and F_{i-r}. Using the equilibrium of forces in the z direction (F_{rez}):

$$F_z = F_{rez} + P_{zeix} - P_{zrols} - P_{zrets} - F_{i-r} = 0 \quad \rightarrow \quad F_{rez} = 22.72\ N \tag{7}$$

In the 3D printed supports (Figure 6.b), the shaft reaction forces are described in the square geometry as F_V e F_h. The F_h is the reaction to F_{rey}, so $|F_h| = F_h = 3.98\ N$.

The F_{ch} is related to the force exerted by the pairs of magnets, interacting with all other surrounding magnetic

elements. F_{ch} is resulted from the aluminum plate that keeps them fixed to the 3D printed support. From the analysis performed in *femm*, this force equals to$|F_{ch}| = F_{ch} = 234.65\ N$, being distributed evenly on the two surfaces illustrated in figure 8(a).

The force due to the weight of the magnets is described as F_{p-ima}, with a mass of $0.3\ kg$ ($|F_{p-ima}| = 2.94\ N$). The force in the *z* direction, F_V, is equivalent to the contact reaction with the shaft, ($|F_V| = F_V = 22.72\ N$).

4. STRUCTURAL ANALYSIS OF 3D PRINTED PIECES

A structural analysis was carried out to verify the dimensioning of the components in order to avoid mechanical failures or malfunctions due to excessive displacement that could affect the alignment of the components. The structural simulation performed by the SolidWorks software, aimed to analyze the maximum Von Mises stresses and maximum displacements in each component. The weight force of each component was obtained from the component's volume and density, using SOLIDWORKS software. For the components printed in 3D, the density of ABS ($1.04 \times 10^3\ \frac{kg}{m^3}$) was used (3DLAB, 2021), while for Gadolinium the density of $7900\frac{kg}{m^3}$ was used.

Table 1. Forces exerted on the System.

Element (Mechanical Interaction)	**Force (**N**)**
Gear (weight)	$1.22\ (-z)$
2 Gd sectors (weight)	$2.47\ (-z)$
2 Bearing	$F_{zrols} = 0.43\ (-z)$
2 Gasket	$F_{zrets} = 0.01\ (-z)$
Shaft	$F_{zeix} = 0.48\ (-z)$
Magnets-bearing force	$F_{i-r} = 21.80\ (-z)$
Repulsion Force between Pairs of Magnets	$F_7 = 348\ (+x\ and\ -x)$
Resistance Force (Friction + Magnetic)	$8.71\ (F_1)$

On the gear, the contact area to the bearings was fixed. The applied forces were: F_1, F_{i-sG} and F_m (Figure 5b). On the shaft, the contact region to the 3D printed supports were fixed while the applied forces were: two times the F_{rol} and two times the F_{rt}(Figure 5.a). On the 3D printed support, the lower surface was rigidly fixed, while the applied forces were: F_7, F_{ch}, F_v, F_h and F_{p-mag} (Figure 6b). At all analyses, all forces were applied as uniformly distributed loads normal to the interfaces with the other components. The material properties for the printed ABS were obtained by works in the literature (Silva, 2019).

To define the safety factor, the empirical methodology proposed by Collins (2019) was used. The methodology is based on eight penalty factors related to different design considerations: (i) accuracy of estimated efforts; (ii) accuracy of the estimated stresses; (iii) relevance of the failure criterion in relation to the chosen material; (iv) necessity to reduce material weight and cost; (v) severity of consequences in case of failure; (vi) quality of workmanship; (vii) operating condition and; (viii) inspection and maintenance quality.

Table 2. Structural mechanical analysis parameters (Silva, 2019).

Parameters	**Valor**
Poisson's Ratio	0.38
Elastic Module	$2.6\ GPa$
Yield Stress	$7.17\ MPa$
Ultimate Stress	$7.65\ MPa$

For each one parameters, a value from -4 to $+4$ was assumed. The higher the value adopted, the greater the safety factor. A penalty factor of 3was chosen for the first criterion, since the contact efforts were simplified as uniformly distributed loads. Criteria (ii) and (iii) were chosen as 3, since parts are produced by additive manufacturing, and the finite element simulation assumes that the material is isotropic and homogeneous. The pejorative factor of 1 was used for criterion (vi), since 3D printing does not have as accurate surface finish as a machined part.

As there are no serious risks in case of failure, nor need for maintenance, the other criteria had a penalty factor of zero, having no influence on the safety factor value. Thus, for the design of the magnetic cooler, the sum of the penalties was

$t = 10$. Continuing with the methodology proposed by Collins, $Nd = 1 + \frac{(10+t)^2}{100}$, for $t > -6$. Then, $Nd = 5$.

The yield stress, as mentioned, is 7.1 MPa. So, 1.43 MPa as the allowable design stress.

To ensure that the mesh discretization had no influence on the results, a second simulation with a more refined mesh was performed in all simulations. At least twice as many elements were used, ensuring that the maximum Von Mises Stress difference between the used mesh and refined one was always inferior to 1.5 %.

Maximum Von Mises Stress and displacements are presented in table 3 and figure 7. Gear and shaft design demonstrated stresses below the allowable design stresses. The 3D printed support presented stresses lower than the material Yield stress, however they were higher than the allowable design stress. A new geometry for this component will be proposed before the refrigerator´s construction.

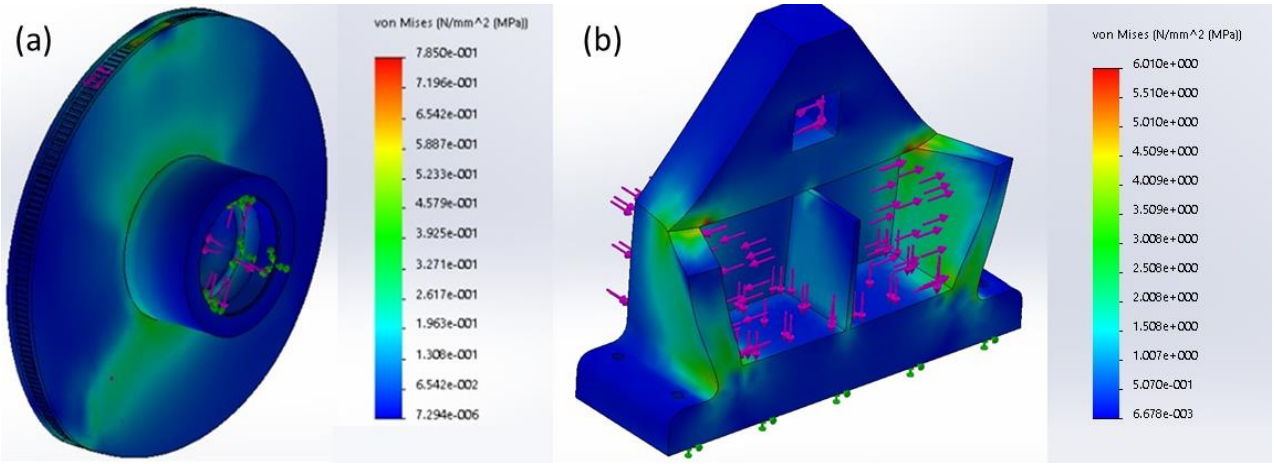

Figure 7. (a) Representation of Von Mises Stresses on the Gear (b) Representation of Von Mises Stresses in the Bearing

Table 3. Results from FE analysis

Component	**Maximum Von Mises Stress (MPa)**	**Maximum displacement ($10^{-3}\ m$)**	**Number of elements**
Gear	0.78	lower than 0.02	33 thousand
Shaft	0.31	lower than 0.01	12.8 thousand
3D printed supports	6.01	0.155	9.5 thousand

5. CONCLUSIONS

With all the challenges faced regarding materials and manufacturing processes for the base elements of the project, the results reached our expectations. For the friction and magnetic force tests against the movement of the acquired stepper motor, the dimensions did not exceed the limits of the motor, ensuring good functioning of the rotary system. As for the leak test, the seal withstood no leakage up to the maximum design pressure, which uses a water pump with a maximum pressure of 30 KPa. The Von Mises stresses of the adapted elements did not exceed the allowable stress for the shaft and gear, while the 3D printed supports will need to be redesigned, seeing the high magnetic separation forces between the used magnets. After this adaptation, future steps for this project will consist in the construction and evaluation of the prototype.

6. ACKNOWLEDGEMENTS

The authors would like to thank the Brazilian agencies CNPq and FAPERJ for financial support. This study was financed in part by the Coordenação de Aperfeiçoamento de Pessoal de Nível Superior - Brasil (CAPES) - Finance Code 001.

7. REFERENCES

Albertini, F., Bennati, C., Bianchi, M., Branchini, L. Cugini, F., Pascale, A. De, Fabbrici, S., Melino, F., Ottaviano, S., Peretto, A., Rosati, J., and Solzi, M., 2017. “Preliminary Investigation on a Rotary Magnetocaloric Refrigerator Prototype, Energy”. *Procedia*, Vol. 142, pp. 1288–1293.

Anitha, R., Arunachalam, S., Radhakrishnan, P., 2001. “Critical Parameters Influencing the Quality of Prototypes”. *Fused Deposition Modelling in Journal of Materials Processing Technology*, Vol. 118, 385-388.

Benhadid-Dib, S., and Benzaoui, A., 2012. “Refrigerants and their Environmental Impact Substitution of Hydro Chlorofluorocarbon HCFC and HFC Hydro Fluorocarbon. Search for an Adequate Refrigerant”. *Energy Procedia*, Vol. 18, pp. 807–816.

Calm, J. M., 2002. “Emissions and environmental impacts from air-conditioning and refrigeration systems”. *International Journal of Refrigeration*, Vol. 25, No. 3, pp. 293–305.

Collins, J. A., Busby, H., Staab, G., 2019. Projeto Mecânico de Elementos de Máquinas. 2ª ed. LTC.

Dankov, S. Yu., Tishin, A. M., Pecharsky, V. K., and Gschneidner. K.A., 1998. “Magnetic phase transitions and the magnetothermal properties of gadolinium”. *Physical Review B*, Vol. 57, No. 6, pp. 3478–3490.

Dias, F. W. R., 2011, “Comportamento mecânico do polímero PTFE sujeito a diferentes taxas de deformação”, Dissertação de Mestrado. Niterói. Rio de Janeiro, Brasil. Universidade Federal Fluminense.

Divyathej, M. V., Varun, M., Rajeev, P., 2016. “Analysis of Mechanical Behavior of 3D Printed ABS Parts by Experiments”. *International Journal of Scientific & Engineering Research*, Vol. 7(3). ISSN 2229-5518.

Galina, D. M., Garcia, D. P., Souza, G. G., Silva, L. R. R., Maziero R., 2016. “Caracterización de las propiedades mecánicas de los cuerpos de prueba ABS confeccionados con diferentes parámetros de extrusión vía impresión 3D”. *Revista Iberoamericana de Polímeros*, Vol. 17(6), 303-309.

Gschneidner, K. A., and Pecharsky, V. K., 2008. “Thirty years of near room temperature magnetic cooling: Where we are today and future prospects”. *International Journal of Refrigeration*, Vol. 31, No. 6, pp. 945–961.

Huang, B., Lai, J. W., Zeng, D. C., Zheng, Z. G., Harrison, B., Oort, A., Dijk, N. H. van, and Brück, E., 2019. “Development of an experimental rotary magnetic refrigerator prototype”. *International Journal of Refrigeration*, Vol. 104, pp. 42–50.

Kitanovski, A., Tušek, J., Tomc, U., Plaznik, U., Ozbolt, M., and Poredoš, A., 2015. “Magnetocaloric Energy Conversion: From Theory to Applications”. *Springer International Publishing (Green Energy and Technology).*

Kurek, A. P., Sellin, N., Gelsleichter, M., 2009. “Redução e substituição do ácido crômico na etapa de condicionamento de ABS para metalização”. Polímeros: Ciência e Tecnologia, Vol. 19(3), 248-254.

Martinez, A. C. P., Souza, D. L. de, Santos, D. M. dos, Pedroti, L. G., Carlo, J. C., Martins, M. A. D., 2019. “Avaliação do comportamento mecânico dos polímeros ABS e PLA em impressão 3D visando simulação de desempenho estrutural”. *Gestão & Tecnologia De Projetos*, Vol. 14(1), 125-141.

NEOMOTION, “Datasheet de produto motores de passo. Datasheet, Grupo Neyoama. Joinville. 3DLAB. Disponível em: <https://3dlab.com.br/como-saber-se-o-filamento-e-abs-ou-pla/> . Acesso em 10/06/2021.

Shang, G., Sun, C., 2020. “Effect of 3D Printing Technology on 3C Product Manufacturing”. *World Journal of Engineering and Technology*, Vol. 8, 712-719.

Silva, F. L. F., 2019. “Comissionamento e estudo dos materiais PLA e ABS processado através da manufatura aditiva.” Relatório final de Iniciação Científica, Faculdade de Tecnologia de Sorocaba. Sorocaba, p.33, 2019.

Smith, A., 2013. “Who discovered the magnetocaloric effect?”. *The European Physical Journal H*, Vol. 38, No. 4, pp. 507–517.

Szykiedans, K., Credo, W., Osiński, D., 2017. “Selected Mechanical Properties of PETG 3D Prints in XXI International Polish-Slovak Conference”. *Machine Modeling and Simulations in Procedia Engineering*, Vol. 177, 455-461.

Tishin, A. M., and Spichkin, Y. I., 2003. “The Magnetocaloric Effect and Its Applications”. CRC Press.

Tishin, A. M., and Spichkin, Y. I., 2014. “Recent progress in magnetocaloric effect: Mechanisms and potential applications". *International Journal of Refrigeration*, Vol. 37, pp. 223–229.

Tušek, J., Samo, Z., Šarlah, A., Prebil, I., and Poredoš, A., 2010. “Development of a rotary magnetic refrigerator”. *International Journal of Refrigeration*, Vol. 33, No. 2, pp. 294–300.

Vuarnoz, D., Kitanovski, A., Gonin, C., Egolf, P. W., and Kawanami, T., 2011. “Modeling and Simulation of the Operation of a Rotary Magnetic Refrigerator”. *Journal of Thermal Science and Technology*, Vol. 6, No. 1, pp. 21–33.

Wittbrodt, B. T., Glover, A. G., Laureto, J., Anzalone, G. C., Oppliger, D., Irwin, J. L., Pearce, J. M., 2013. “Life-cycle economic analysis of distributed manufacturing with open-source 3-D printers”. *Mechatronics*, Vol. 23(6), 713-726.

8. **RESPONSIBILITY NOTICE**

The authors are the only responsible for the printed material included in this paper.